Meteorologische Zeitschrift, Vol. **17**, No. 5, 613-620 (October 2008)

Article

A new algorithm for the extraction of cloud parameters using multipeak analysis of cloud radar data – First application and preliminary results

SABRINA MELCHIONNA[1*], MATTHIAS BAUER[2], and GERHARD PETERS[3]

[1]Max-Planck-Institute for Meteorology, Hamburg, Germany
[2]METEK GmbH, Elmshorn, Germany
[3]Meteorological Institute, University of Hamburg, Germany

(Manuscript received February 14, 2008; in revised form July 18, 2008; accepted July 18, 2008)

Abstract

Spectral and polarimetric signatures of echoes, obtained with a vertically pointing millimeter wave radar, are examined with regard of their potential to retrieve range resolved microphysical characteristics of clouds, including the detection of mixed phases. A novel target classification algorithm based on this information was applied to deep frontal clouds. Examples of spectral/polarimetric profiles are shown to illustrate the retrieval technique, and first findings on microphysical structures and dynamics of such cloud systems are presented.

Zusammenfassung

Spektrale und polarimetrische Signaturen von Echos, die man mit einem vertikal gerichteten Millimeterwellen Radar erhält, werden in Hinblick auf die Möglichkeiten untersucht, hieraus höhenaufgelöste mikrophysikalische Wolkeneigenschaften einschließlich der Detektierung gemischter Phasen abzuleiten. Ein neuer Zielklassifizierungs-Algorithmus, der diese Signaturen nutzt, wurde auf hochreichende frontale Wolken angewendet. An Hand von Beispielen spektral/polarimetrischer Profile werden die Retrieval-Technik und erste Ergebnisse zu mikrophysikalischen Strukturen und der Dynamik solcher Wolkensysteme gezeigt.

1 Introduction

In the past decade cloud radars in the millimeter wave range have emerged as a powerful tool for cloud observation (CLOTHIAUX et al., 1995; KROPFLI and KELLY, 1996; MORAN et al., 1998; KOLLIAS et al., 2005). In particular parameters related to the small scale variability of clouds, which is not resolved by models but which is important in determining the radiative effects of clouds, have been shown to be extractable from cloud radar data (HOGAN and ILLINGWORTH, 2000). Long term programs like ARM (http://www.arm.gov/) or CLOUDNET (see ILLINGWORTH et al. (2007), for a comprehensive review and further references) have rendered possible the quantification of climatological cloud parameters. The representation of cloud parameters in the regional model REMO was studied by HENNEMUTH et al. (2008), using data from cloud radar, water vapor DIAL, and other auxiliary observations.

Radar wavelengths from 3 to 10 mm are particularly suited for the observation of clouds and drizzle. While the longer waves are less affected by attenuation, they suffer more than shorter waves from undesired cross sensitivity to non-meteorological targets like insects and seeds (atmospheric plankton) or birds which tend to appear in the atmospheric boundary layer during the warm season. Surprisingly, the detection threshold for small cloud droplets (although a key parameter of cloud radars), is not important criterion for choice of the wavelength within the mentioned wavelength range, because the dependence of the scattering cross section on wavelength (proportional to λ^{-4}) is about compensated by increasing available transmit power and receiver sensitivity with increasing wavelength. In this study a wavelength at the upper end of the useful range ($\lambda = 8.3$ mm) was used due the superior capability in penetrating deep precipitating clouds. While the scattering cross section of cloud droplets is proportional to λ^{-4}, the scattering cross section of atmospheric plankton with size comparable to the radar wavelength is only weakly dependent on λ. Therefore an efficient atmospheric plankton detection algorithm is more important at $\lambda = 8.3$ mm than at shorter wavelengths.

While radar have unique capabilities to retrieve cloud morphology, the quantitative retrieval of microphysical parameters is more difficult (GOSSARD et al., 1997; MATROSOV et al., 2001), and the use of multiple wavelengths and/or the combination with other available information is most promising for such task. Concepts of such integrated systems are considered in detail in RUFFIEUX and FURGER (2006), or in LOEHNERT et al. (2007). Nevertheless, the success of any sensor combination depends largely on how well and to which extent

*Corresponding author: Sabrina Melchionna, Max-Planck-Institute for Meteorology, Bundesstrasse 53, 20146 Hamburg, Germany, e-mail: sabrina.melchionna@zmaw.de

DOI 10.1127/0941-2948/2008/0322

0941-2948/2008/0322 $ 3.60

the information provided by each particular sensor is understood and exploited.

Here we consider Doppler spectra received with a vertically pointing cloud radar in the co- and cross-polarized plane. The relation between co- and cross-polarized backscatter cross-section, termed LDR (Linear Depolarization Ratio), is an indicator for the shape of the scattering particles. For spherical particles, as cloud- or drizzle-drops, LDR is zero. Therefore, any deviation of LDR from zero is an indicator for the presence of non-spherical particles in the scattering volume. Note that LDR can be calculated only when at the same height level both co- and cross- signals are present. Normally the cross-signal is lower than the co-signal, up till, especially for cloud particles, it can not even be detected; in this case LDR is not calculable.

Conventionally, the first three moments of Doppler spectra (power, Doppler velocity and spectral width) are used to retrieve microphysical cloud parameters, as characteristic particle size (GOSSARD et al., 1997) or liquid/ice water content (LIAO and SASSEN, 1994; GAUSSIAT et al., 2003). Sometimes these three moments are not sufficient to describe the complex structure of observed spectra. KOLLIAS et al. (2001), demonstrated how turbulence parameters can be retrieved in raining clouds from spectral echo structures, which are not included in the three-moment characterization of Doppler spectra. Also in this study additional features of the Doppler spectra are analyzed with the aim to extract more detailed information on the microphysical structure and on the kinetics in clouds.

A peak detection algorithm has been developed, by which the Doppler spectra are decomposed into multiple peaks. Each peak is parametrized by a set of three peak-specific spectral moments and in addition, if possible, by the peak-specific LDR.

Moreover, on this basis hydrometeors are efficiently separated from "non-meteorological" echoes (BAUER and GOERSDORF, 2007), in particular from atmospheric plankton, which can be the dominating signal in the atmospheric boundary layer.

2 Instrument and data processing

A 36 GHz Doppler research vertically pointing cloud radar, MIRA-36, operates in Hamburg, Germany. The radar characteristics are summarized in Table 1. Among the measurements collected between September 2006 and July 2007, we examined closely spectra from several days in which deep frontal clouds showed up. For these clouds the spectral width - conventionally evaluated - showed large values, typical of mixed-phase clouds.

The Doppler spectra of a vertically pointing cloud radar is determined by the velocities and scattering cross sections of various kinds of particles. These include primarily droplets, ice crystals and other suspended particles often referred to as atmospheric plankton. The

Table 1: Radar operational parameters

Parameter	Value
Frequency	36 GHz
Peak power	30 kW
Pulse length	200 ns
Pulse repetition frequency	5kHz
Range resolution	30 m
Diameter of the antenna	1.2 m
Beamwidth	0.52 °
Sensitivity at 5 km	-44 dBZ
Minimum detectable LDR	-40 dB
FFT length	256
Integration time	10 ns

Doppler velocity observed for any particle depends on one hand on particle properties controlling the sedimentation velocity, namely their mass and aerodynamic drag, and on the other hand on the vertical velocity of the ambient air. This ambiguity must be taken into consideration in any attempt to interpret Doppler spectra in terms of particle characteristics (see appendix for further discussion).

The receiver noise floor of every Doppler spectrum is determined using the method of HILDEBRAND and SEKHON (1974). The spectral powers, corrected for noise, were transformed into the logarithmic domain before applying the multiple peak detection algorithm.

For illustration of the performance of the peak detection algorithm, spectra with height dependent structure are displayed in Figure 1 for selected altitudes of different measurement times. The shaded area shows the measured spectrum. In case of multiple peaks, the dashed lines represent the decomposition into individual Gaussian peaks, while the solid line show the spectrum as reconstructed from the decomposition. In Figure 1a one narrow peak is close to zero velocity, which is typical for small ice particles or cloud droplets. In Figure 1b two narrow peaks are partially overlapping, that can be caused by coexisting habits of small cloud-forming hydrometeors. In Figure 1c one peak has center fall velocity and width much enhanced compared to the peaks of the first two panels. The height level of this peak was below the melting layer and the shape of the spectrum is typical for light rain fall. The fidelity of the Gaussian fit is only moderate here, because it cannot account for the skewness of the spectrum, which is typical for rain. The skewness is due to the fact that the Doppler velocity is proportional to the 6^{th} moment of particle diameter. Hence bigger raindrops, although their concentration in rainfalls is low, mostly contribute to the backscattering cross section of the radar resolution volume (see appendix). In Figure 1d the rain spectrum is split into two modes, which can be explained as a consequence of drop size sorting.

When the cloud spectra as the one in Figure 1b are described only by the conventional three global mo-

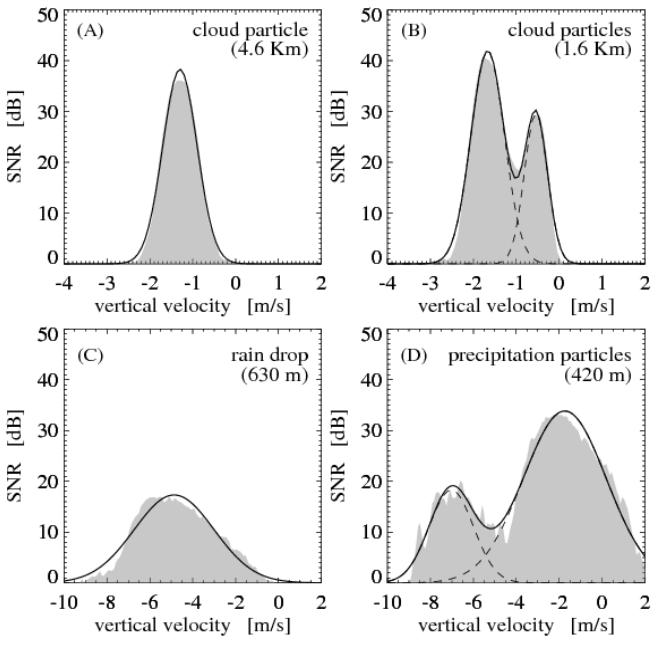

Figure 1: Example of different structures of Doppler spectra. Negative velocities are downwards. Shaded areas: measurements; dashed lines: decomposition into Gaussian peaks; solid lines: reconstruction of spectrum from decomposition. In case of single peak, solid and dashed lines obliviously overlap. Note the different vertical velocity scales among the panels. Panel (a): 2007.01.18 03:26:20 UTC. Panel (b): 2007.03.01 02:11:40 UTC. Panel (c): 2007.01.28 09:12:10 UTC. Panel (d): 2007.01.31 13:42:50 UTC.

ments, essential elements of the spectra are missed, leading to erroneous retrievals.

The rationale for detecting and separating spectral peaks is the assumption that the Doppler spectra can be represented by a linear superposition of Gaussian distributions (termed "modes" in the following), every mode being produced by a discrete class of hydrometeors with characteristic fall velocities.

If only one class of meteorological targets exists in the radar sample volume, then a Gaussian curve is generally a good fit for the spectrum. If, instead, the radar sample volume contains two classes of meteorological targets, the linear superposition of two Gaussian curves may be used to describe the spectrum. To separate analytically the cases, we consider first the hypothesis that the spectrum consists of one mode, and we calculate the square mean difference between the measured spectrum and the single Gaussian fit. Our single mode hypothesis is correct if this difference is lower than an opportune threshold. The threshold is selected after eye inspection of samples of many spectra profiles, taken from clouds showing different vertical and temporal extension or different values of the first three conventional moments.

It also turned out that the decomposition in up to two modes is adequate in most cases except of moderate or strong rain which is beyond the scope of this study. The basic inadequacy of Gaussian fits in rain is foreshadowed in Figure 1c. Moreover, spectra with stronger skewness tend to result in a decomposition into multiple but physically meaningless modes.

When two Gaussian curves fit the data, an additional criterion of separability is applied: two peaks are considered to represent separate modes when the distance between their centers is greater than the mean value of their standard deviations. If is not so, the spectrum is fitted again with one Gaussian curve only.

Our hypothesis is that every peak corresponds to a mode and that every mode corresponds to one class of cloud particles, which evolve descending to the surface. If it would be possible to establish a relation within modes along the height range, we could improve our understanding of evolution and of phase transformations for the particles constituting a mode.

In order to identify mode profiles on the height range, we performed a cluster analysis. For every vertical profile, the spectra are considered stepping downward starting from the highest height level. If only one peak is present, it is always assigned to a primary mode. If two peaks are present, the primary mode is associated with that peak whose velocity is closest to the velocity of the primary mode in the next higher range gate. It follows that the primary mode is the one with larger vertical extension. The above described procedures are applied to the co- and cross-channels separately.

Examples of profiles of decomposed spectra for drizzling clouds are shown in Figure 2. For every range gate every mode of the fitted Doppler spectrum is depicted by the mode-specific mean velocity (black ticks), by the mode-specific standard deviation (colored horizontal bars), and by the mode-specific peak value profile (right side of the plots). The colors of the standard deviation bars indicate the modes. The co- and cross-channels are shown in the left and right panels respectively. The melting layer can be recognized by the associated jump of velocity.

3 Results

3.1 Mixed-Phase structures

The peak detection algorithm often reveals, among the cases until now analyzed, well separated dual modes above the melting layer. These structures may reach from the melting layer to hundreds of meters above it (Fig. 2b and 2c), or may cover the whole cloud depth. Their temporal persistence may range up to one hour. Dual modes, present along the cloud above the melting layer, can sometimes extend into the rain range (Fig. 2b). Following the considerations of ZAWADZKI et al. (2001), it is reasonable to consider this structure due to the coexistence in the same sampling volume of either cloud supercooled droplets and snow flakes, or of different crystal habits.

Another occasionally observed double structure is the generation of a "branch", hung on the left (higher

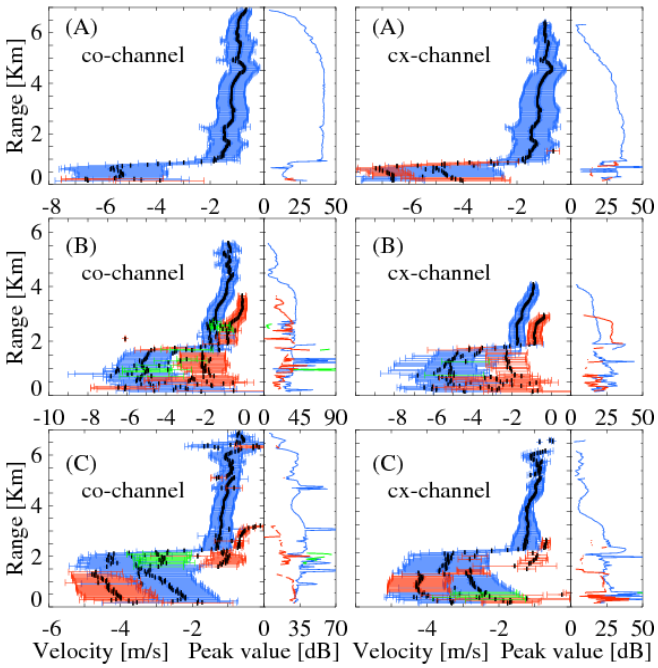

Figure 2: Examples of decomposed Doppler spectra profiles. (a) 2007.01.20 00:41:20 UTC; (b) 2007.03.18 03:25:30 UTC; (c) 2007.04.24 03:55:30. Left panels: co-channel; right panels: cross-channel. On the left side of every panel the mode-specific velocity (with negative velocities downwards) is depicted by black ticks, and the mode-specific standard deviation by colored horizontal bars; the colors indicate the mode order number: blue for the primary mode, red for the secondary mode, green for the third mode (physically probably meaningless). On the right side of every panel the mode-specific peak value profiles are depicted by correspondingly colored lines. Note the different velocity and peak value scales of the panels.

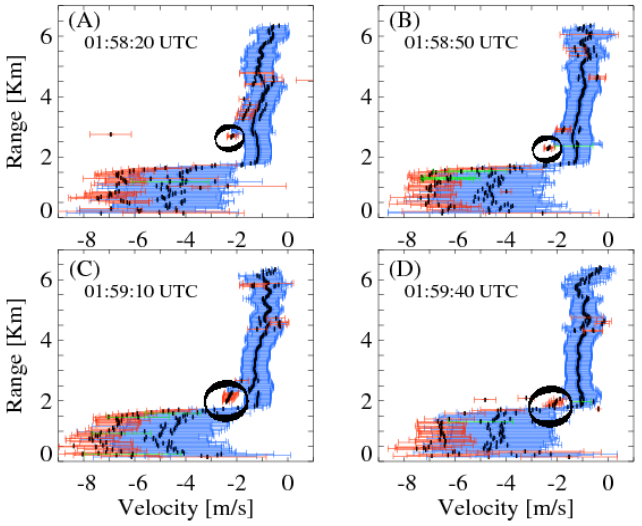

Figure 3: Sequence of co-channel spectra profiles, 2007.03.18 01:58 UTC. A secondary mode with higher fall velocity, forming a branch (black circle) from the primary mode, emerges at about 3 km (panel a) and disappears in the melting layer at about 2 km (panel d). A time of about 70 s elapsed between panel (a) and (d) .

falling velocity) with respect of the primary mode (Fig. 3, black circles). This secondary mode, no more than 500 meters in vertical range extension, falls fast, and disappears in the melting layer after some minutes.

3.2 Calculation of LDR

The mode-specific LDR ensues from dividing the mode-specific peak value in the cross-channel by the mode-specific peak value in the co-channel. Due to the much lower signal-to-noise ratio in the cross-channel a bimodal distribution observed in the co-channel only rarely can be observed also in the cross-channel. Figure 4 shows one example of these favorable cases, in which it is possible to calculate mode-specific LDR for both primary mode and secondary mode. The LDR-values observed above the melting layer between 1 and 2 km are significantly mode dependent: most LDR-values are below 0 dB for the primary mode (blue stars) and above –2 dB for the secondary mode (red stars). This sharp separation in LDR values in a 1 km depth above the melting layer suggests the existence of two ice crystal habits or of a mixed phase, composed by droplets and ice crystals. This conclusion agrees with several studies analyzing mixed-phase cloud with different instruments as SHUPE et al. (2004); HUDAK et al. (2002); KOROLEV et al. (2003).

Moreover, the gradually increasing LDR values and, at the same time, the gradually increasing falling velocity values for the primary mode between 2 and 3.5 km, may be explained as the result of growing hydrometeors.

3.3 Vertical mean velocity

Another result obtained by the mode decomposition, concerns vertical structures in clouds. Figures 2 to 4 show that the Doppler velocity is directed downward and tends to increase while approaching the cloud base. In order to analyze this behavior more systematically we consider only the primary mode and fit, with a least absolute deviation method, the mode-specific velocity values to a linear dependence on the vertical range. Figures 5a and 5b show examples of the linear fit for a drizzling and a non-precipitating cloud, respectively. The vertical range for the fit extends from 1.5 km up to the cloud top. The lower bound of 1.5 km was chosen in order to include data only from above the melting layer in case of raining clouds.

In Figures 6a and 6b we show two periods of two hours duration with persistent deep frontal clouds up to 8 km. The first period refers to a drizzling/raining cloud while the second period refers to a non-precipitating cloud with cloud base descending from 4 to 1.8 km. The analysis of time series of the fitted profiles revealed that the mean velocity gradient assumes a fairly constant value with a mean value of about $0.14 \cdot 10^{-3}$ s^{-1} (that is 14 cms^{-1} per kilometer fall path).

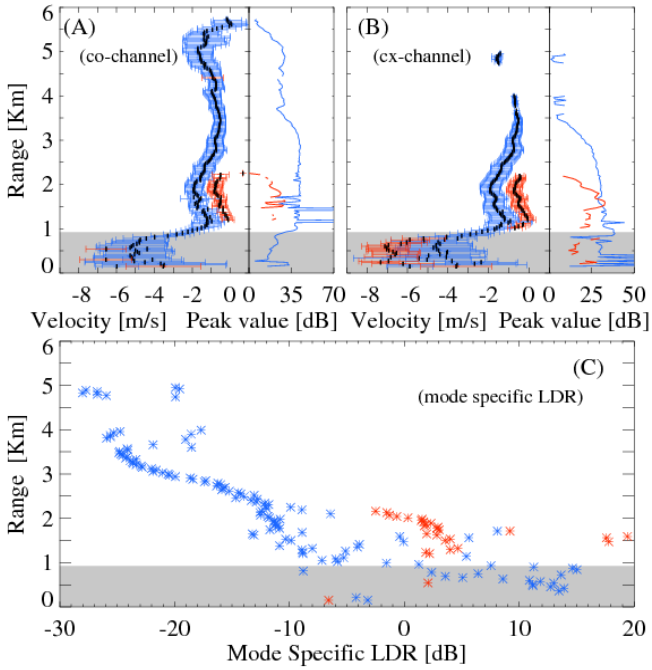

Figure 4: Upper panels: bimodal profile between 1 and 2 km. (a): co-channel. (b): cross-channel. Lower panel (c): mode-specific LDR values observed between 1 and 2 km. The mode specific LDR is evaluated dividing the mode specific peak value in the cross-channel to the mode specific peak value in the co-channel. The colors correspond to the modes in the upper panels. The shaded area highlights the raining zone, below the melting layer. 2007.03.01 02:11:40 UTC.

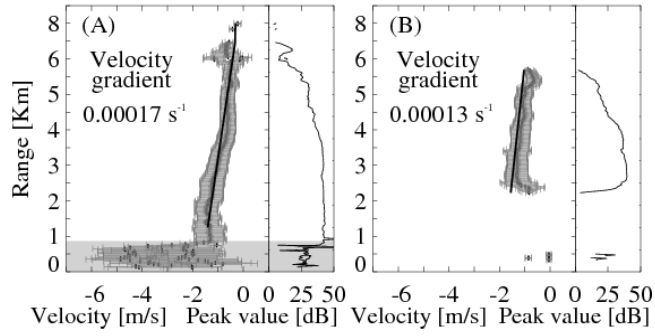

Figure 5: Linear fit of vertical profile of the primary mode-specific falling velocity. The range for the fit extends between the melting layer and cloud top. Only spectra profile in the co-channel are considered. (a) Example for a raining cloud spectra profile; 2007.03.01 00:32:30 UTC. (b) Example for a non-raining cloud spectra profile, 2007.01.18 01:19:50 UTC.

Time series of the mean velocity gradient for the two cases showed in Figures 6a and 6b are respectively in Figures 7a and 7b. This mean gradient represents roughly 360 profiles per hour, every profile consisting on the average of at least 500 range gates. At a first glance the downward direction of the Doppler velocity is surprising, because the mean vertical wind within active clouds should be directed upward with fast enough

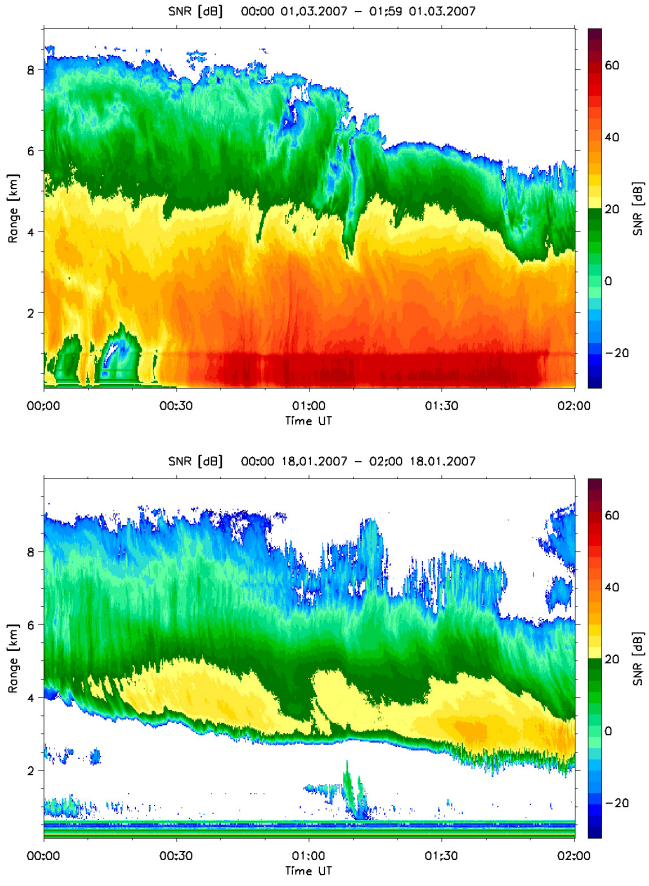

Figure 6: Time height cross-sections for SNR (signal to noise ratio) profiles for: upper panel 2007.03.01 00:00-02:00 UTC, height range from 0 to 9 km; lower panel 2007.01.18 00:00-02:00 UTC, height range from 0 to 10 km.

speed to carry cloud droplets upward, thus inducing their growth by condensation. We explain the observed downward velocity with the very strong weighting of large hydrometeors in the radar echo (proportional to the 6^{th} power of the diameter). Therefore the Doppler velocity is dominated by those hydrometeors which had been grown on their upward travel by a sufficient amount that their terminal fall velocity exceeds the updraft of ambient air. As we can observe only the superposition of updraft and terminal fall velocity, we cannot infer any quantitative statement on the particle size directly from the Doppler velocity. Nevertheless, the increasing Doppler velocity on the fall path can be explained as the consequence of particle-growth due to various microphysical interaction processes occurring on the encounter of other hydrometeors existing on the fall path. We believe that the observed (and fairly stable) velocity gradient could represent a useful parameter to be taken into consideration for the validation of modeling of related microphysical processes.

Deviations from this behavior appear close to the cloud top (in Fig. 5a at about 5.7 km), where turbulence is enhanced due to radiative cooling, or in case of non-

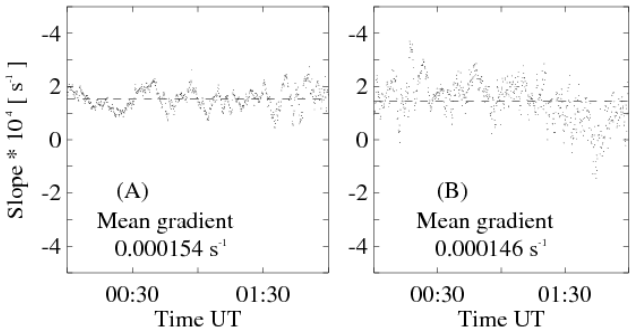

Figure 7: Time series for the vertical mean velocity gradient in the clouds of fig. 6. The dots represent single estimates of the gradient and the dashed line indicates the mean value along the corresponding observation period. (a) 2007.03.01 00:00-02:00 UTC; (b) 2007.01.18 00:00-02:00 UTC.

raining clouds in a narrow layer close to the cloud base, where an abrupt inversion of this gradient is often observed (Fig. 5b).

4 Conclusions and outlooks

The results presented here, demonstrate that the multipeak analysis of Doppler spectra can help to improve our knowledge of microphysical processes in clouds. The described multiple peak detection algorithm, including peak specific LDR, turns out to be a promising tool to extract information, particularly on mixed-phase clouds. The analysis of echoes from deep frontal clouds yielded the following preliminary results:

1. Doppler spectra above the melting layer frequently split up into two modes. In such cases it is occasionally possible to determine mode-specific values of LDR, which indicate the existence of mixed phases or separate habits of ice crystals;

2. the deep frontal clouds analyzed showed a linear fall velocity (first spectral moment) profile between melting layer and cloud top with velocity amplitudes decreasing with increasing height;

3. in non-precipitating clouds, and if no melting layer is visible, the range of constant velocity gradient extended from about 1 km above cloud base to the cloud top. In the lower 1 km of the cloud layer an inverted gradient and Doppler velocity approached zero at the cloud base were observed;

4. close to the cloud top a range of enhanced turbulence is observed, which is apparently a consequence of radiation induced instability.

If further measurements confirm that the observed vertical velocity gradient in clouds is of general validity, it should be reproducible by cloud resolving models with explicit microphysics. Also the observation of coherent multiple peak structures in the spectra profile can be useful for model validation.

5 Appendix: Doppler spectra of particles in the presence of turbulence

Following WAKASUGI et al. (1986) the Doppler spectrum $S(w)$ of a radar echo from particles in turbulent air can be expressed by:

$$S(w) = PS_p(w - \overline{w}) * S_t(w) \qquad (5.1)$$

with w Doppler velocity, P echo power, $S_p(w)$ reflectivity weighted pdf of the particle sedimentation velocity in still air, $\overline{w}$ vertical velocity of the ambient air averaged over the spatial and temporal radar resolution intervals (henceforth called mean wind) and $S_t(w)$ spatial and temporal pdf of the unresolved vertical velocity within the radar resolution intervals (henceforth called turbulence). The asterix stands for the convolution operator. Wakasugi et al. analyzed the case of simultaneous scattering at particles and at turbulent refractive index variations. Since we can safely exclude the last scattering mechanism for the cloud radar wave length, we adopted a simplified version of their equation.

While there is no general solution to retrieve the undisturbed Doppler signature $PS_p(w)$ of the particle population there are special cases, in which certain particle properties can be inferred. We will consider here those hypothetical cases, which are invoked in the later interpretation of observed spectra.

5.1 Negligible particle sedimentation velocity

Here $S_p(w)$ is a delta-function, which peaks at $w = 0$. Then eq.(5.1) assumes the form

$$S(w) = P\delta(-\overline{w}) * S_t(w) = PS_t(w - \overline{w}) \qquad (5.2)$$

The spectral distribution is entirely determined by the mean and turbulent air velocity. The particles are perfect tracers of the air motion. This is assumed to be a good description for example of the echoes from atmospheric plankton, because averaging of $\overline{w}$ over long time intervals ($>$ several hours) yields a vanishing mean velocity for this type of echoes. This is just to be expected for the vertical wind component in the boundary layer and could hardly be generated by particles with any noticeable sedimentation velocity. Generally the pdf S_t of the turbulence and S_m of the mean wind is adequately described by normal distributions:

$$S_t(w - \overline{w}) = (2\pi\sigma_t^2)^{-\frac{1}{2}} \exp\left(\frac{(w - \overline{w})^2}{2\sigma_t^2}\right) \qquad (5.3)$$

$$S_m(\overline{w}) = (2\pi\sigma_m^2)^{-\frac{1}{2}} \exp\left(\frac{\overline{w}^2}{2\sigma_m^2}\right) \qquad (5.4)$$

The radar spectrum is described completely by three moments, namely P, $\overline{w}$ and σ.

Usually the relation $\sigma_m > \sigma_t$ holds in the atmosphere as a consequence of the "red" shape of turbulence spectra in the inertial subrange.

5.2 Measurable mean sedimentation velocity $\overline{w_p}$ but small width σ_p of $S_p(w)$

In many cases (cloud drops, ice crystals, small drizzle droplets) the mean sedimentation velocity $\langle w_p \rangle$ cannot be neglected ("$\langle\ \rangle$" denotes here reflectivity weighted averaging over the particle size distribution). Nevertheless, it is assumed that the width of the reflectivity weighted velocity distribution σ_p, which is related to the size distribution of the particles, is still smaller than σ_t or least than σ_m . In this case the approximation for equation (5.1) reads:

$$\begin{aligned} S(w) &= P\delta(-\overline{w} - \langle w_p \rangle) * S_t(w) \\ &= P S_t(w - \overline{w} - \langle w_p \rangle) \end{aligned} \qquad (5.5)$$

The generally observed Gaussian shape of $S(w)$ suggests that velocity distribution is dominated by convolution with turbulence, although some additional broadening due to the sedimentation velocity distribution cannot be excluded. At the same time the long term averaging of the first moment is influenced or may be even dominated by $\langle w_p \rangle$. Indeed, long term averages of Doppler velocities of cloud echoes have a consistent downward bias. In view of the general picture that the mean air motion in clouds should be upward the sedimentation velocity must be dominating. A quantitative separation of both contributions is nevertheless not possible without further information.

5.3 Two or multiple spectral peaks with Gaussian shape and similar width

Inspection of equation (5.1) shows how multiple peaks can possibly be generated. The turbulence term $S_t(w)$ is assumed to follow a Gaussian distribution. Even, if we allow for some deviation from this model – e.g. due to buoyancy induced skewness – there is hardly a turbulence process imaginable which would exhibit multimodal velocity distributions. Multiple peaks on the other hand can easily be explained by the first term $S_p(w-\overline{w})$. If there are different classes of particles, they may yield Doppler spectra with separated peaks, provided that the convolution with turbulence does not merge adjacent peaks. If the widths $\sigma_{p,i}$ are small compared to σ_t, the approximate form of equation (5.1) reads:

$$S(w) = \sum_i P_i \delta(w - \overline{w} - \langle w_{p,i} \rangle) * S_t(w) \qquad (5.6)$$

According to the distributive law the convolution can be applied to each peak separately, showing that each peak exhibits the same width, namely σ_t. Vice versa, the occurrence of multiple peaks with similar width and shape suggests, that their spectral width is dominated by turbulence and that the widths $\sigma_{p,i}$ are smaller than σ_t. A necessary condition for the separability of adjacent peaks is that $|\langle w_{p,i} \rangle - \langle w_{p,i+1} \rangle| > \sigma_t$. Another important conclusion, which can be inferred from equation (5.6), is that the observed velocity differences of multiple peaks are not dependent on turbulence or mean wind $\overline{w}$. All peaks are shifted by the same mean wind. The physical assumption behind this expectation is that acceleration effects can be neglected. BOHNE (1982) analyzed the incomplete response of hydrometeors to turbulent acceleration. It was shown to be noticeable for large rain drops but negligible for small hydrometeors, which are in the focus of this paper.

5.4 Skewed peaks and multiple peaks with different width

As turbulence typically shows a Gaussian velocity distribution skewed spectra can be considered as indication for $S_p(w)$ dominating the observed spectral shape.

The fall velocity of rain drops can attain several ms^{-1} depending on their size. The size distribution is usually described by an exponential function or modified gamma-function and the corresponding two values of $\langle w_p \rangle$ and σ_p are comparable or typically larger than $\overline{w}$ and σ_t respectively. In the latter case equation (5.1) can be approximated by:

$$S(w) = P S_p(w) \propto \sigma_B(D) N(D) \left(\frac{\partial w(D)}{\partial D}\right)^{-1} \qquad (5.7)$$

with $\sigma_B(D)$ single particle backscatter cross section, $N(D)$ drop size distribution and $w(D)$ terminal fall velocity. The impact of vertical wind on the interpretation of rain spectra was discussed by PETERS et al. (2005). With increasing size the fall velocity of rain drops increases but reaches a saturation value at $w_{\max} \approx 9.7\,\mathrm{ms}^{-1}$ (ATLAS et al., 1973). Therefore $(\partial w/\partial D)^{-1}$ approaches very high values for $w \to w_{\max}$. For rain rates larger than 0.5 mmh^{-1} there is usually a sufficient number of drops with $w \approx w_{\max}$ causing $S(w)$ to exhibit a maximum close to $w_{\max}$, i.e. at the upper edge of the spectrum. Consequently spectra of moderate or stronger rain show a skewed shape. Usually it is not possible to observe simultaneous echoes of cloud droplets and rain due to the overwhelming strength of rain echoes. Light drizzle on the other hand may be observed together with cloud droplets and the drizzle may sometimes form a separate Doppler peak with some greater width than the cloud peak because of the drizzle fall velocity distribution. The shape of the drizzle peak is typically Gaussian since the above mentioned spectral enhancement at $w_{\max}$ does not take effect due to the lack of large drops.

References

ATLAS, D., R.C. SRIVASTA, R.S. SEKHON, 1973: Doppler radar characteristics of precipitation at vertical incidence. – Rev. Geophy. **11**, 1–35.

BAUER, M.R., U.GOERSDORF, 2007: Target separation and classification using cloud radar doppler-spectra. – In: 33rd AMS Conference on Radar Meteorology, Cairns, Australia.

BOHNE, A.R., 1982: Radar detection of turbulence in precipitation environments. – J. Atmos. Sci. **39**, 1819–1837.

CLOTHIAUX, E.E., M.A. MILLER, B.A. ALBRECHT, T.P. ACKERMAN, J. VERLINDE, D.M. BABB, R.M. PETERS, W.J. SYRETT, 1995: An evaluation of a 94-ghz radar for remote-sensing of cloud properties. – J. Atmos. Ocean. Technol. **12**, 201–229.

GAUSSIAT, N., H. SAUVAGEOT, A.J. ILLINGWORTH, 2003: Cloud liquid water and ice content retrieval by multiwavelength radar. – J. Atmos. Ocean. Technol. **20**, 1264–1275.

GOSSARD, E.E., J.B. SNIDER, E.E. CLOTHIAUX, B. MARTNER, J.S. GIBSON, R.A. KROPFLI, A.S. FRISCH, 1997: The potential of 8-mm radars for remotely sensing cloud drop size distributions. – J. Atmos. Ocean. Technol. **14**, 76–87.

HENNEMUTH, B., A. WEISS, J. BOSENBERG, D. JACOB, H. LINNE, G. PETERS, S. PFEIFER, 2008: Quality assessment of water cycle parameters in REMO by radar-lidar synergy. – Atmos. Chem. Phys. **8**, 287–308.

HILDEBRAND, P.H., R.S. SEKHON, 1974: Objective determination of noise-level in doppler spectra. – J. Appl. Meteor. **13**, 808–811.

HOGAN, R.J., A.J. ILLINGWORTH, 2000: Deriving cloud overlap statistics from radar. – Quart. J. Roy. Meteor. Soc. **126**, 2903–2909.

HUDAK, D., B. CURRIE, P. RODRIGUEZ, S.G. COBER, I. ZAWADZKI, G.A. ISAAC, 2002: Cloud phase detection in winter stratiform clouds using polarimetric doppler radar. – In: Proceedings of the Second European Conference on Radar Meteorology (ERAD), 90–94.

ILLINGWORTH, A.J., R.J. HOGAN, E.J. O'CONNOR, D. BOUNIOL, M.E. BROOKS, J. DELANOE, D.P. DONOVAN, J.D. EASTMENT, N. GAUSSIAT, J.W.F. GODDARD, M. HAEFFELIN, H.K. BALTINK, O.A. KRASNOV, J. PELON, J.M. PIRIOU, A. PROTAT, H.W.J. RUSSCHENBERG, A. SEIFERT, A.M. TOMPKINS, VAN G.J. ZADELHOFF, F. VINIT, U. WILLEN, D.R. WILSON, C.L. WRENCH, 2007: Cloudnet – continuous evaluation of cloud profiles in seven operational models using ground-based observations. – Bull. Amer. Meteor. Soc. **88**, 883–898.

KOLLIAS, P., B.A. ALBRECHT, R. LHERMITTE, A. SAVTCHENKO, 2001: Radar observations of updrafts, downdrafts, and turbulence in fair-weather cumuli. – J. Atmos. Sci. **58**, 1750–1766.

KOLLIAS, P., E.E. CLOTHIAUX, B.A. ALBRECHT, M.A. MILLER, K.P. MORAN, K.L. JOHNSON, 2005: The atmospheric radiation measurement program cloud profiling radars: An evaluation of signal processing and sampling strategies. – J. Atmos. Ocean. Technol. **22**, 930–948.

KOROLEV, A.V., G.A. ISAAC, S.G. COBER, J.W. STRAPP, J. HALLETT, 2003: Microphysical characterization of mixed-phase clouds. – Quart. J. Roy. Meteor. Soc. **129**, 39–65.

KROPFLI, R.A., R.D. KELLY, 1996: Meteorological research applications of mm-wave radar. – Meteor. Atmos. Phys. **59**, 105–121.

LIAO, L., K. SASSEN, 1994: Investigation of relationships between Ka-band radar reflectivity and ice and liquid water contents. – Atmos. Res. **34**, 231–248.

LOEHNERT, U., VAN E. MEIJGAARD, H.K. BALTINK, S. GROSS, R. BOERS, 2007: Accuracy assessment of an integrated profiling technique for operationally deriving profiles of temperature, humidity, and cloud liquid water. – J. Geophys. Res. Atmos. **112**(D4).

MATROSOV, S.Y., R.F. REINKING, R.A. KROPFLI, B.E. MARTNER, B.W. BARTRAM, 2001: On the use of radar depolarization ratios for estimating shapes of ice hydrometeors in winter clouds. – J. Appl.d Meteor. **40**, 479–490.

MORAN, K.P., B.E. MARTNER, M.J. POST, R.A. KROPFLI, D.C. WELSH, K.B. WIDENER, 1998: An unattended cloud-profiling radar for use in climate research. – Bull. Amer. Meteoro. Soc. **79**, 443–455.

PETERS, G., B. FISCHER, H. MUNSTER, M. CLEMENS, A. WAGNER, 2005: Profiles of raindrop size distributions as retrieved by microrain radars. – J. Appl. Meteor. **44**, 1930–1949.

RUFFIEUX, D.E., M. FURGER, 2006: Special issue cost 720 tuc. – Meteorol. Z. **15**, 3–97.

SHUPE, M.D., P. KOLLIAS, S.Y. MATROSOV, T.L. SCHNEIDER, 2004: Deriving mixed-phase cloud properties from doppler radar spectra. – J. Atmos. Ocean. Technol. **21**, 660–670.

WAKASUGI, K., A. MIZUTANI, M. MATSUO, S. FUKAO, S. KATO, 1986: A direct method for deriving drop-size distribution and vertical air velocities from VHF doppler radar spectra. – J. Atmos. Ocean. Technol. **3**, 623–629.

ZAWADZKI, I., F. FABRY, W. SZYRMER, 2001: Observations of supercooled water and secondary ice generation by a vertically pointing x-band Doppler radar. – Atmos. Res. **59-60**, 343–359.